Title
Non-invasive terahertz imaging of tissue water content for flap viability assessment.

Journal
Biomedical Optics Express, 8(1)

ISSN
2156-7085

Authors
Bajwa, Neha
Au, Joshua
Jarrahy, Reza
et al.

Publication Date
2017

DOI
10.1364/boe.8.000460

Peer reviewed

Research Article | Vol. 8, No. 1 | 1 Jan 2017 | BIOMEDICAL OPTICS EXPRESS 460
Biomedical Optics EXPRESS

Non-invasive terahertz imaging of tissue water content for flap viability assessment

Neha Bajwa,[1,*] Joshua Au,[2] Reza Jarrahy,[3] Shijun Sung,[4] Michael C. Fishbein,[5] David Riopelle,[1] Daniel B. Ennis,[1,6] Tara Aghaloo,[2] Maie A. St. John,[2] Warren S. Grundfest,[1,4,7] and Zachary D. Taylor[4,7]

[1]*Department of Bioengineering, University of Los Angeles, California (UCLA), 410 Westwood Plaza, Los Angeles, CA 90025, USA*
[2]*Department of Head and Neck Surgery, UCLA, 200 Medical Plaza, Los Angeles, CA 90025, USA*
[3]*Department of Plastic Surgery, UCLA, California, 200 Medical Plaza, Los Angeles, CA 90025, USA*
[4]*Department of Electrical Engineering, UCLA, 410 Westwood Plaza, Los Angeles, CA 90025, USA*
[5]*Department of Pathology and Laboratory Medicine, UCLA, 200 Medical Plaza, Los Angeles, CA 90025, USA*
[6]*Department of Radiological Sciences, UCLA, 300 Medical Plaza, Los Angeles, CA 90025, USA*
[7]*Department of Surgery, UCLA, California, 200 Medical Plaza, Los Angeles, CA 90025, USA*
[*]*nbajwa1@gmail.com*

Abstract: Accurate and early prediction of tissue viability is the most significant determinant of tissue flap survival in reconstructive surgery. Perturbation in tissue water content (TWC) is a generic component of the tissue response to such surgeries, and, therefore, may be an important diagnostic target for assessing the extent of flap viability *in vivo*. We have previously shown that reflective terahertz (THz) imaging, a non-ionizing technique, can generate spatially resolved maps of TWC in superficial soft tissues, such as cornea and wounds, on the order of minutes. Herein, we report the first *in vivo* pilot study to investigate the utility of reflective THz TWC imaging for early assessment of skin flap viability. We obtained longitudinal visible and reflective THz imagery comparing 3 bipedicled flaps (i.e. survival model) and 3 fully excised flaps (i.e. failure model) in the dorsal skin of rats over a postoperative period of 7 days. While visual differences between both models manifested 48 hr after surgery, statistically significant ($p < 0.05$, independent t-test) local differences in TWC contrast were evident in THz flap image sets as early as 24 hr. Excised flaps, histologically confirmed as necrotic, demonstrated a significant, yet localized, reduction in TWC in the flap region compared to non-traumatized skin. In contrast, bipedicled flaps, histologically verified as viable, displayed mostly uniform, unperturbed TWC across the flap tissue. These results indicate the practical potential of THz TWC sensing to accurately predict flap failure 24 hours earlier than clinical examination.

OCIS codes: (110.0110) Imaging systems; (170.0170) Medical optics and biotechnology; (170.6795) Terahertz imaging.

References and links

1. J. R. Payette, E. Kohlenberg, L. Leonardi, A. Pabbies, P. Kerr, K.-Z. Liu, and M. G. Sowa, "Assessment of Skin Flaps Using Optically Based Methods for Measuring Blood Flow and Oxygenation," Plast. Reconstr. Surg. **115**(2), 539–546 (2005).
2. M. Bergkvist, J. Henricson, F. Iredahl, E. Tesselaar, F. Sjöberg, and S. Farnebo, "Assessment of microcirculation of the skin using Tissue Viability Imaging: A promising technique for detecting venous stasis in the skin," Microvasc. Res. **101**, 20–25 (2015).
3. L. Di Sieno, G. Bettega, M. Berger, C. Hamou, M. Aribert, A. D. Mora, A. Puszka, H. Grateau, D. Contini, L. Hervé, J.-L. Coll, J.-M. Dinten, A. Pifferi, and A. Planat-Chrétien, "Toward noninvasive assessment of flap viability with time-resolved diffuse optical tomography: a preclinical test on rats," J. Biomed. Opt. **21**(2), 025004 (2016).

#275156 http://dx.doi.org/10.1364/BOE.8.000460
Journal © 2017 Received 2 Sep 2016; revised 4 Dec 2016; accepted 5 Dec 2016; published 23 Dec 2016

Biomedical Optics EXPRESS

4. Q. Yang, Z. H. Ren, D. Chickooree, H. J. Wu, H. Y. Tan, K. Wang, Z. J. He, C. J. Gong, V. Ram, and S. Zhang, "The effect of early detection of anterolateral thigh free flap crisis on the salvage success rate, based on 10 years of experience and 1072 flaps," Int. J. Oral Maxillofac. Surg. **43**(9), 1059–1063 (2014).
5. K.-T. Chen, S. Mardini, D. C.-C. Chuang, C.-H. Lin, M.-H. Cheng, Y.-T. Lin, W.-C. Huang, C.-K. Tsao, and F.-C. Wei, "Timing of presentation of the first signs of vascular compromise dictates the salvage outcome of free flap transfers," Plast. Reconstr. Surg. **120**(1), 187–195 (2007).
6. G. S. Lazarus, D. M. Cooper, D. R. Knighton, R. E. Percoraro, G. Rodeheaver, and M. C. Robson, "Definitions and guidelines for assessment of wounds and evaluation of healing," Wound Repair Regen. **2**(3), 165–170 (1994).
7. C. Holm, M. Mayr, E. Höfter, A. Becker, U. J. Pfeiffer, and W. Mühlbauer, "Intraoperative evaluation of skin-flap viability using laser-induced fluorescence of indocyanine green," Br. J. Plast. Surg. **55**(8), 635–644 (2002).
8. I. A. Pestana, B. Coan, D. Erdmann, J. Marcus, L. S. Levin, and M. R. Zenn, "Early Experience with Fluorescent Angiography in Free-Tissue Transfer Reconstruction," Plast. Reconstr. Surg. **123**(4), 1239–1244 (2009).
9. M. F. Stranc, M. G. Sowa, B. Abdulrauf, and H. H. Mantsch, "Assessment of tissue viability using near-infrared spectroscopy," Br. J. Plast. Surg. **51**(3), 210–217 (1998).
10. M. G. Sowa, J. R. Payette, and H. H. Mantsch, "Near-infrared spectroscopic assessment of tissue hydration following surgery," J. Surg. Res. **86**(1), 62–69 (1999).
11. W. Eichhorn, T. Auer, E.-D. Voy, and K. Hoffmann, "Laser Doppler imaging of axial and random pattern flaps in the maxillo-facial area. A preliminary report," J. Craniomaxillofac. Surg. **22**(5), 301–306 (1994).
12. F. Arnold, C. F. He, C. Y. Jia, and G. W. Cherry, "Perfusion imaging of skin island flap blood flow by a scanning laser-Doppler technique," Br. J. Plast. Surg. **48**(5), 280–287 (1995).
13. Y.-S. Jin, G.-J. Kim, and S.-G. Jeon, "Terahertz dielectric properties of polymers," (2006).
14. P. H. Siegel, "Terahertz technology in biology and medicine," in *Microwave Symposium Digest, 2004 IEEE MTT-S International* (2004), **Vol. 3**, p. 1575–1578.
15. N. Bajwa, B. Nowroozi, S. Sung, J. Garritano, A. Maccabi, P. Tewari, M. Culjat, R. Singh, J. Alger, W. Grundfest, and Z. Taylor, "Reflective THz and MR imaging of burn wounds: a potential clinical validation of THz contrast mechanisms," in (2012), Vol. 8496, p. 84960X–84960X–7.
16. Z. D. Taylor, R. S. Singh, D. B. Bennett, P. Tewari, C. P. Kealey, N. Bajwa, M. O. Culjat, A. Stojadinovic, H. Lee, J.-P. Hubschman, E. R. Brown, and W. S. Grundfest, "THz medical imaging: in vivo hydration sensing," IEEE Trans. Terahertz Sci. Technol. **1**(1), 201–219 (2011).
17. P. Tewari, C. P. Kealey, D. B. Bennett, N. Bajwa, K. S. Barnett, R. S. Singh, M. O. Culjat, A. Stojadinovic, W. S. Grundfest, and Z. D. Taylor, "In vivo terahertz imaging of rat skin burns," J. Biomed. Opt. **17**(4), 040503 (2012).
18. Z. D. Taylor, J. Garritano, S. Sung, N. Bajwa, D. B. Bennett, B. Nowroozi, P. Tewari, J. W. Sayre, J.-P. Hubschman, S. X. Deng, and others, "THz and mm-Wave Sensing of Corneal Tissue Water Content: In Vivo Sensing and Imaging Results," Terahertz Sci. Technol. IEEE Trans. On **5**, 184–196 (2015).
19. Z. D. Taylor, J. Garritano, S. Sung, N. Bajwa, D. B. Bennett, B. Nowroozi, P. Tewari, J. Sayre, J.-P. Hubschman, S. Deng, E. R. Brown, and W. S. Grundfest, "THz and mm-Wave Sensing of Corneal Tissue Water Content: Electromagnetic Modeling and Analysis," IEEE Trans. Terahertz Sci. Technol. **5**(2), 170–183 (2015).
20. B. B. Hu and M. C. Nuss, "Imaging with terahertz waves," Opt. Lett. **20**(16), 1716 (1995).
21. W. A. Dorsett-Martin, "Rat models of skin wound healing: a review," Wound Repair Regen. **12**(6), 591–599 (2004).
22. G. Deyoung, R. A. Henry, and R. M. McFarlane, "The design of a pedicle flap in the rat to study necrosis and its prevention," Plast. Reconstr. Surg. **35**(2), 177–182 (1965).
23. P. N. Manson, R. M. Anthenelli, M. J. Im, G. B. Bulkley, and J. E. Hoopes, "The role of oxygen-free radicals in ischemic tissue injury in island skin flaps," Ann. Surg. **198**(1), 87–90 (1983).
24. S. Richard, B. Querleux, J. Bittoun, O. Jolivet, I. Idy-Peretti, O. de Lacharriere, and J.-L. Leveque, "Characterization of the Skin In Vivo by High Resolution Magnetic Resonance Imaging: Water Behavior and Age-Related Effects," J. Invest. Dermatol. **100**(5), 705–709 (1993).
25. G. M. Gordillo and C. K. Sen, "Revisiting the essential role of oxygen in wound healing," Am. J. Surg. **186**(3), 259–263 (2003).
26. "Skin graft survival on avascular defects.: Plastic and Reconstructive Surgery," http://journals.lww.com/plasreconsurg/Fulltext/1975/01000/SKIN_GRAFT_SURVIVAL_ON_AVASCULAR_DEFECTS_.10.aspx.
27. J. Burge, "Essentials of Plastic Surgery – Second Edition. Edited by J. E. Janis. St. Louis, MO/Boca Raton, FL: PB - QMP/CRC Press, 2014. 1336 pages. Paperback. ISBN: 978-1-57626-385-3. Price: $AUD132.00.," ANZ J. Surg. **84**, 981–982 (2014).
28. M. Attas, M. Hewko, J. Payette, T. Posthumus, M. Sowa, and H. Mantsch, "Visualization of cutaneous hemoglobin oxygenation and skin hydration using near-infrared spectroscopic imaging," Skin Res. Technol. **7**(4), 238–245 (2001).
29. J. M. Converse, J. Smahel, D. L. Ballantyne, Jr., and A. D. Harper, "Inosculation of vessels of skin graft and host bed: A fortuitous encounter," Br. J. Plast. Surg. **28**(4), 274–282 (1975).

Biomedical Optics EXPRESS

1. Introduction

Tissue "flaps" have become essential for the surgical reconstruction of patients with breast cancer, head and neck cancer, large soft tissue defects, and wounds [1,2]. A flap includes the harvested skin, muscle, soft tissue or bone, and their corresponding neurovascular supply. This tissue is surgically resected and rotated or transferred from a donor site to a recipient site [3]. Patency of the underlying arteries and veins is vital for flap survival. In cases of vascular occlusion (i.e. thrombosis), flap outcome directly correlates with the rapid restoration of the vessels' patency; if reduced viability can be identified before 6 hr of thrombosis onset, which typically occurs within 72 hr following surgery, 60 - 73% of compromised flaps may be salvaged [4,5].

The current gold standard for determining flap viability is clinical examination, in which skin color, capillary refill, turgor, and bleeding patterns are periodically examined [1,3,6]. This method, however, is highly operator-dependent, and changes in the appearance of the flap due to microvascular complications are generally delayed by 1 to 2 hours, thus preventing early intervention [3]. Efforts towards achieving more non-invasive and accurate tissue viability measurements have been widespread and include the use of several adjunctive technologies.

One such method is fluorescent angiography that uses exogenous fluorophores to measure tissue perfusion in flaps [7,8]. Because of physiological shortcomings associated with the tracer substance, specifically a long half-life and diffusion into the interstitium, repeated assessments consistent with current clinical monitoring practice are difficult [7]. Near-infrared diffuse reflectance spectroscopy and visible light spectroscopy have both been investigated for assessing tissue viability by measuring hemoglobin oxygenation and hemoglobin concentration [9]. However, these are all one-point measurements subject to excessive sampling error and are, therefore, not suited to monitor large flap areas. Since the chances of recovery after occlusion are directly proportional to the rapidity of diagnosis of the entire flap area, rapid, non-invasive *imaging* of a physiological indicator of tissue viability may be more appropriate for flap assessment.

Among the available flap imaging techniques, such as laser Doppler imaging, variation in tissue water content (TWC) - an acute manifestation of injury as well as a significant parameter in the evaluation of skin health- is a major confounder to measurement of flap perfusion during the acute phase following surgery [10–12]. Reflective terahertz (THz) imaging, however, uses TWC to generate native, pathology-specific tissue contrast in 2D reflection images; the dielectric properties of water at THz frequencies (100 GHz to 10 THz range) yield easily detectable increases in THz reflectivity for small increases in hydration, lending TWC as an effective contrast mechanism in reflective THz imaging *in vivo* [13–15]. Our group has previously reported on the use of a novel, reflective THz imaging system to non-invasively detect and longitudinally monitor TWC in cornea and burn wounds *in vivo* [16–19]. Reflective THz imaging is also unique in that it I) employs safe, low power non-ionizing radiation [16]; II) probes the bulk properties of superficial tissue using simple, optics-based measurements [13,14,16,20]; III) and is minimally perturbed by hair and even some types of medical dressings [14,16].

Here, we aim to perform THz imaging of myocutaneous flaps in a pre-clinical rat model to explore the utility of THz-TWC based maps for early flap viability assessment. Six myocutaneous flaps of either high tissue viability (n = 3) or low tissue viability (n = 3) were surgically created in the dorsal skin of rats and a previously reported reflective THz imaging system was used to track the distribution of TWC across the flap margin over a period of 7 days [15–17]. This time window was selected based on morphological changes observed in the field of view (FOV) and motivated by the evolution of the wound healing response following cutaneous injury [3]. Rats were selected as our pre-clinical model given thicknesses of rat and human skin layers are most similar compared to those of other animal models (i.e. pig, mouse, and hairless mouse) [21]. A survey of the literature also shows the rat model has

Biomedical Optics EXPRESS

proven useful for studying changes in skin subsequent to surgical elevation of a dorsal skin flap [10]. A 2.5 x 2.5 cm^2 excised myocutaneous flap and a 2.5 x 2.5 cm^2 bipedicled myocutaneous flap were selected as a failure and survival model, respectively [22]. We hypothesized that a flap model of lower tissue viability would present lower TWC contrast, and therefore its THz map would display reduced THz reflectivity with respect to that of uninjured skin. Reflective THz measurements of skin were compared to temporally and spatially matched histology and clinical assessments.

2. Reflective THz imaging system

As shown in Fig. 1(a), a reflective THz imager, which measures 12 cm x 10 cm x 8 cm, was used to acquire TWC maps of myocutaneous flaps. The THz source, receiver electronics, and system design have been previously reported and are, therefore, summarized below [16]. The THz system operates in reflection mode at a center frequency of 0.525 THz with ~125 GHz bandwidth. The effective center frequency and bandwidth of the system are constrained by the THz source's power spectral density and the detector's spectral responsivity. As reported in our

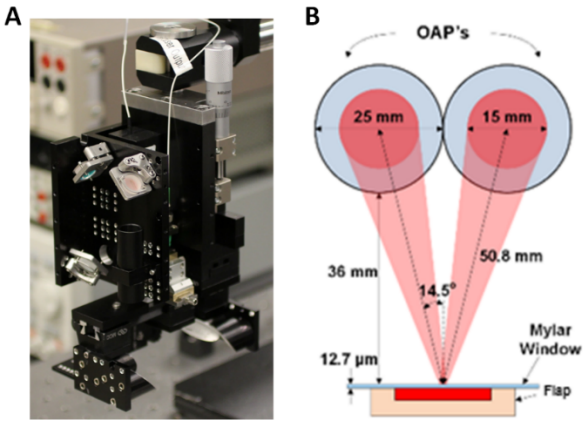

Fig. 1. *In vivo* THz imaging system. (a) Visible image of the reflective THz system. Dorsal flaps of anesthetized rats are raster scanned on x- and y-stepper motors beneath the imager. The encirlcled optics correspond to (b) off-axis parabolic (OAP) mirrors used to focus the THz beam onto a thin-film Mylar window that serves to mitigate surface contours of the underlying flap.

previous *in vivo* THz imaging work, this bandwidth is sufficient to overcome speckle and is sensitive to changes in tissue water content with good spatial resolution [16]. The photoconductive switch (PCS) based THz source is pumped by a 780 nm pulse train created by a frequency-doubled 1550 nm mode-locked laser with a 230 fs pulse width and 20 MHz repetition frequency. The resulting THz source beam is collimated by a 76.2 mm effective focal length (EFL), 25.4 mm clear aperture off-axis 90° parabolic (OAP) mirror. As shown in Fig. 1(b), a 50.8 mm EFL OAP mirror at a 14° incidence angle is used to focus the beam onto the target. The reflected THz radiation is then collected and collimated by a second 50.8 mm EFL OAP. Finally, a 25.4 mm EFL OAP couples the collected signal to the feedhorn of a WR1.5 waveguide mounted Zero-bias Schottky diode detector (ZBSD). THz pulses are rectified by the ZBSD and then amplified with 38 dB of gain with a low-noise broadband amplifier. Resulting THz signals are coupled to a gated receiver driven with a reference pulse generated using a beam sampler, 1550-nm high-speed photodiode, and RF pulse amplifier. The THz imaging system acquires pixel-by-pixel data with a 1 ms integration time, and an image is generated by raster scanning the animal model beneath a fixed, focused THz beam

Biomedical Optics EXPRESS

using x and y stepper motors. An image with a 6 cm x 6 cm FOV requires a scanning time of ~10 min using a 0.5 mm step size.

3. Tissue flap surgery

All experiments were approved by the Institutional Animal Care and Use Committee (IACUC). Six 14 week old male Lewis rats (Charles River Laboratories, Wilmington, MA) weighing 250 - 300 g were used as pre-clinical models to investigate effects of varying flap tissue viability on TWC maps acquired with reflective THz imaging. Here, myocutaneous dorsal flaps of either low or high tissue viability, as shown in Fig. 2, were compared.

All rats were maintained in temperature-regulated environments (24 °C) on a 12-hr light/dark cycle and housed one pair per cage with soft bedding and a microinsolator cover. Animals underwent general anesthesia with inhaled isoflurane and were placed on a water heating pad for temperature regulation at 37 ± 0.5°C. Each rat was shaved from scapula to pelvis to expose

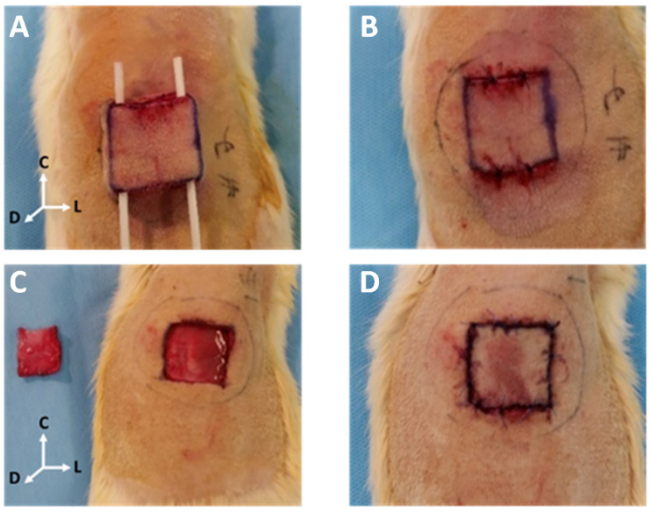

Fig. 2. Myocutaneous flap design. (a) An axially-based bipedicled flap (i.e. survival model), measuring 2.5 x 2.5 cm^2 in area with cephalic and caudal incisions, that is elevated deep to the panniculus carnosous and then (b) surgically secured in its anatomical position. (c) Completely excised myocutaneous skin flap (i.e. failure model), measuring 2.5 x 2.5 cm^2 in area with circumferential flap excision, that is elevated deep to the panniculus carnosous and (d) sutured back in anatomic position. "L," "D," and "C" correspond to lateral, dorsal, and cephalic anatomical directions of the rat.

a 6 x 6 cm^2 area of dorsal skin. Rats were placed in prone position under the THz imaging system, a 12.7 µm dielectric Mylar window was lowered onto the shaved dorsal skin to flatten the imaging field, and pre-evaluation visible and THz images were captured with a SLR camera and the THz imager, respectively. The scanned area of the dorsum was marked with a black marker, and the anesthetized rat was then returned to the surgical field.

The rats were then aseptically prepared with three alternating scrubs of betadine and isopropanol and randomly assigned to receive either a 2.5 x 2.5 cm^2 excisional myocutaneous flap (n = 3) or a bipedicled myocutaneous flap (n = 3).

Shown in Fig. 2(a), the axially based bipedicled mycocutaneous flap was designed as the control for flap survival since all axially based vasculature and the dermal plexus to the flap remained intact through the bipedicled flaps. Using a #15 blade, an incision was made at the cephalic and caudal borders of the designed flap through the panniculus carnosus. The flap was elevated deep to the panniculus carnosous muscular layer to the lateral borders of the

Biomedical Optics EXPRESS

designed flap. Simple interrupted 5-0 polypropylene sutures were used to close the incision in anatomic position as shown in Fig. 2(b).

As shown in Fig. 2(c), the excisional myocutaneous flap was designed as an experimental flap failure since all vasculature was completely ligated when the flap was excised. Using a #15 blade, an incision was made along all borders of the designed flap though the panniculus carnosuos. The flap was elevated deep to the panniculus carnosous muscular layer and the myocutaneous flap was completely excised. The flap was allowed to remain extracorporeal for 20 minutes. Again, simple interrupted 5-0 polypropylene sutures were used to close the incision in anatomic position as shown in Fig. 2(d). Rats were then allowed to recover from anesthesia and transferred to the vivarium for post-operative monitoring. Post-operatively, all animals received analgesia with subcutaneous injections of carprofen (5 mg/kg) daily for 72 hr.

THz and visible imagery were continuously acquired for one hour after surgery, followed by a single 24 hr, 48 hr, and 7-day post-operative scan. At each time point, the dielectric Mylar window was lowered onto the flap during THz imaging. After a 7-day postoperative observation period, the rats were euthanized and histological specimens harvested.

4. Clinical examination

Postoperative monitoring of flap compromise was performed by two head and neck physicians by visual inspection and palpation. Flaps were evaluated on a daily basis for the first 3 days and then finally on day 7 for clinical signs of ischemia and variation in tissue elasticity [1,10]. On postoperative day 7, the total amount of skin flap necrosis was observed and recorded for each rat.

5. Histology design

Figure 3 shows the design used for histological evaluation of both flap viability models. A blind histological analysis of flap tissue harvested at 7 days post operation was compared to visible and THz imagery to determine tissue viability in tissue flaps. A 2 mm x 2 cm region (dotted green rectangle in Fig. 3) was harvested from the cephalic incision sites of each flap, transferred to 10% formalin solution, and submitted for routine processing for histopathological evaluation.

All tissue samples were histologically sectioned saggital to the major axis of the sample and contained an intradermal suture for orientation and registration of the tissue specimen. Three histological slices of 5μm thickness were acquired from each tissue block, stained with hematoxylin and eosin, and analyzed to determine tissue necrosis. Histologic sections included the original flap (i.e. red hatched region under the window in Fig. 3) as well as a myocutaneous margin or non-traumatized tissue (i.e. tan region under the window in Fig. 3) to provide a control area for histologic comparison. Assessment of viability was based on the morphology of the individual cells and patency of vessels [23]. Histological outcome of tissue flaps was compared to visible images, and visible images were compared to their companion THz images. Using this methodology, THz observations were related to histologically verified images of tissue flap viability.

Biomedical Optics EXPRESS

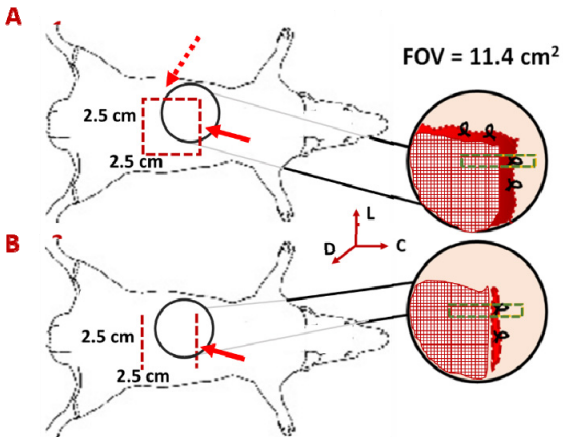

Fig. 3. Histology design. Histological evaluation of tissue viability for (a) an excised flap and (b) a bipedicled flap in a rat imaged under a Mylar window (denoted by the solid black circle). A zoom-in diagram shows the field of view (FOV) of the window, which captures the flap tissue (hatched red region), incisions (solid red lines), and non-traumatized tissue (surrounding tan region. Sagittal histological slices of 5 µm thickness were taken from 2 cm x 2 mm tissue sections (dotted green rectangle) harvested from the cephalic incision site (solid red arrow) on day 7. Dotted red arrow denotes the lateral incision. A suture in each slice (black loop) served as an intradermal fiducial marker for image registration of histology to the same region in the FOV captured by THz-time series imagery. "L," "D," and "C" correspond to anatomical directions detailed in Fig. 2.

6. Statistical analysis

An independent Student *t*-test was used to compare pixel-by-pixel reflectivity differences between pre-surgery and 24hr post-surgery THz images along linear contours for excised flaps and bipedicled flaps. Equal variances were assumed for both flap models and the level of significance was set at $p < 0.05$.

7. Results

7.1 In vivo THz flap imaging

Figure 4 shows *in vivo* THz time-series imagery of three excised flaps (see Fig. 4(a)) and three bipedicled flaps (see Fig. 4(b)) in the dorsal skin of anesthetized rats was acquired over a 7-day period. Skin flaps were imaged under a thin (12 µm) film Mylar window to eliminate confounding effects from non-uniform surface topography, and visible and parallel THz images were generated. Because the dimension of the flaps exceeded that of the dielectric window, only the cephalic incision and flap tissue were captured in THz and visible images. The flap tissue and non-injured area are denoted by grey and yellow fields in visible images at 15min post-surgery, respectively. The "hot" color map associated with THz imagery transforms black to the global minimum THz reflectivity and white to the global maximum THz reflectivity.

During the first 48 hr following surgery, THz reflectivity profiles were generated for 1.5 cm long contours (indicated by white horizontal line segments in THz imagery in Fig. 4) that captured the same region of the cephalic flap margin. Clinical acute assessments of flap viability are typically performed for 48 hours post-operatively, and therefore we used this as our acute endpoint for the THz image analysis [5]. First, THz reflectivity values of these contours were normalized to the maximum THz reflectivity acquired from an aluminum

Biomedical Optics EXPRESS

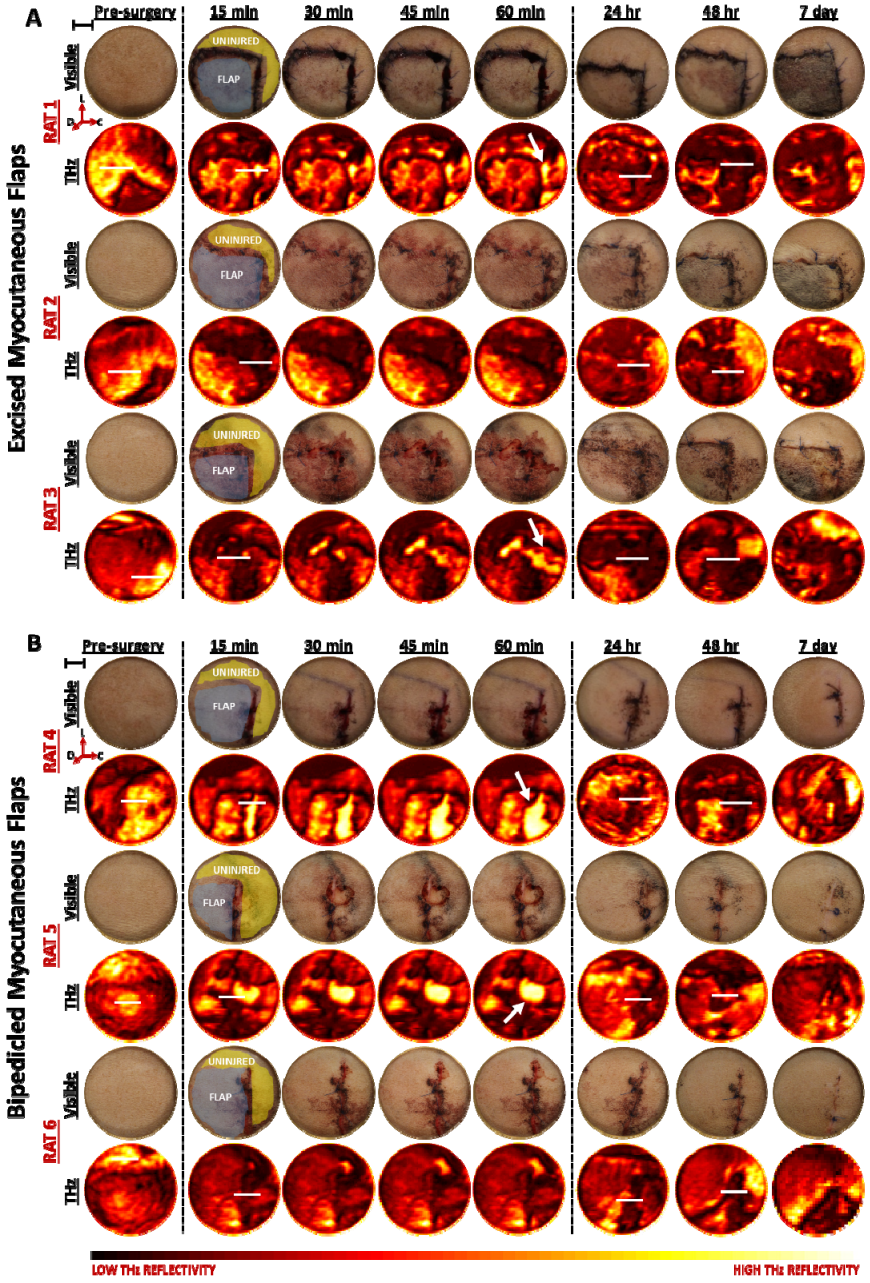

Fig. 4. *In* vivo visible and THz time-series flap imagery. (a) Excised flaps and (b) bipedicled flaps in the dorsum of anesthetized rats were imaged under a 12.7 µm Mylar window over a 7-day period. Uninjured tissue and flap tissue are labeled in yellow and gray fields, respectively, in visible images acquired at 15min following surgery. The hot color map of THz imagery transforms black to the global minimum THz reflectivity and white to the global maximum THz reflectivity. "L," "D," and "C" in the 3D axis denote directions detailed in Fig. 2. Black scale bars represent ~1 cm in the FOV. ~1.5 cm long contours, indicated by solid white horizontal lines, segment the cephalic incision, flap region, and non-traumatized tissue. Solid white arrows locate the leakage of blood, indicated by high THz reflectivity, from the incision site.

Biomedical Optics EXPRESS

calibration target (i.e. ideal reflector) and zero THz reflectivity measured in the absence of a reflecting target (i.e. air). Next, the percent change (% Δ) in THz reflectivity was plotted in Fig. 5, which represents the pixel-by-pixel % reflectivity difference between the different post-surgery THz images (15min, 24hr, and 48hr) and the pre-operative THz image along the white line contour shown in Fig. 4. These reflectivity plots are referred to as "THz profiles." Lengths of the THz profile to the left and right of the cephalic incision site, that is denoted by a dotted vertical line, correspond to the flap region and surrounding non-traumatized tissue, respectively.

As shown in Fig. 4(a) and 4(b), THz images of the rat dorsums prior to flap surgery displayed mostly uniform reflectivity across the FOV. Low reflecting areas, such as those evident in the periphery of many flaps, may have resulted from reduced contact coupling between the Mylar window and underlying skin. Specifically, the curvature of the spine in the dorsal skin of these animal models is hypothesized to have contributed to this effect.

Even with this imaging confounder, THz images for all flaps identified the spatial location of the surgical incisions and flap tissue immediately following surgery. As shown in Fig. 4(a), for THz images of all excised flaps at 15min – 1hr, the flap tissue is characterized by high reflectivity, bordered by a region of low reflectivity (i.e. the cephalic and lateral incision sites), and finally surrounded by region of high reflectivity (i.e. uninjured tissue). This result is most apparent in rat 2, for which little to no blood leakage was observed at the incision site. Similarly, for the bipedicled flap group (see Fig. 4(b)), THz imaging affords the spatial localization of the single cephalic incision. For THz images of most subjects in this group, the incision site appears as a line of low reflectivity bordered by a region of higher reflectivity (i.e. the flap and non-injured tissue). This result is most obvious in rat 6, for which little to no blood leakage was observed at the incision site. Because a bipedicled flap does not include lateral incisions, black lines apparent in THz imagery of this tissue region in Fig. 4(b) were likely due to either intrinsic surface contours within the rat dorsum or dissection borders deep to the panniculus layer rather than gross features from the bipedicled flap. For rat 1, rat 3, rat 4, and rat 5, the leakage of blood (denoted by solid white arrows) from the incision sites further delineated their respective flap margins; blood, like TWC, is a highly reflective, dispersive polar medium, and therefore a confounder to THz TWC contrast. Figure 4 shows the accumulation of blood along the flap margin appears as increased THz reflectivity in all post-op images acquired between 15min and 60min. Even with the presence of blood, the overall reflectivity of the flap region is different between both flap viability groups. Because THz flap imagery acquired 15min postoperatively was least confounded by blood, THz reflectivity at this time point was analyzed for Day 0. THz reflectivity profiles for the aforementioned rats at the 15min mark in Fig. 5 illustrate these irregularities, or "hot spots," along the length of the cephalic incision as clearly defined peaks denoted by solid red arrows. With the exception of these peaks and 'troughs' in the reflectivity plots, likely due to uncoupling between the window and skin and the presence of blood, %Δ THz reflectivity between pre-surgery and 15min post-surgery across the flap for most rats is close to 0%.

Twenty-four hours postoperatively, the contrast of THz images and their accompanying reflectivity profiles became markedly distinct between both flap models. Visible inspection alone of the THz excised flap imagery in Fig. 4(a) suggested reduced THz reflectivity in the form of 'dark zones' at the cephalic and lateral incision site as well as the peripheral segment of the flap. Though reflectivity of the cephalic incision was similarly low in THz imagery of bipedicled flaps, likely due to then dried blood, the surrounding tissue contrast was mostly unperturbed. This result was further substantiated by %Δ THz reflectivity profiles for both flap models at 24hr in Fig. 5(a) and 5(b). A noticeable decline in THz reflectivity (Rat 1: –4%Δ; Rat 2: –4.5%Δ; Rat3: - 5.5%Δ) was apparent in excised flaps (i.e. left of the dotted vertical lines in Fig. 5(a)) which continued to persist by 48hr ensuing surgery in rat 2 and rat 3. Because of the aforementioned coupling issues between the window and underling tissue

Biomedical Optics EXPRESS

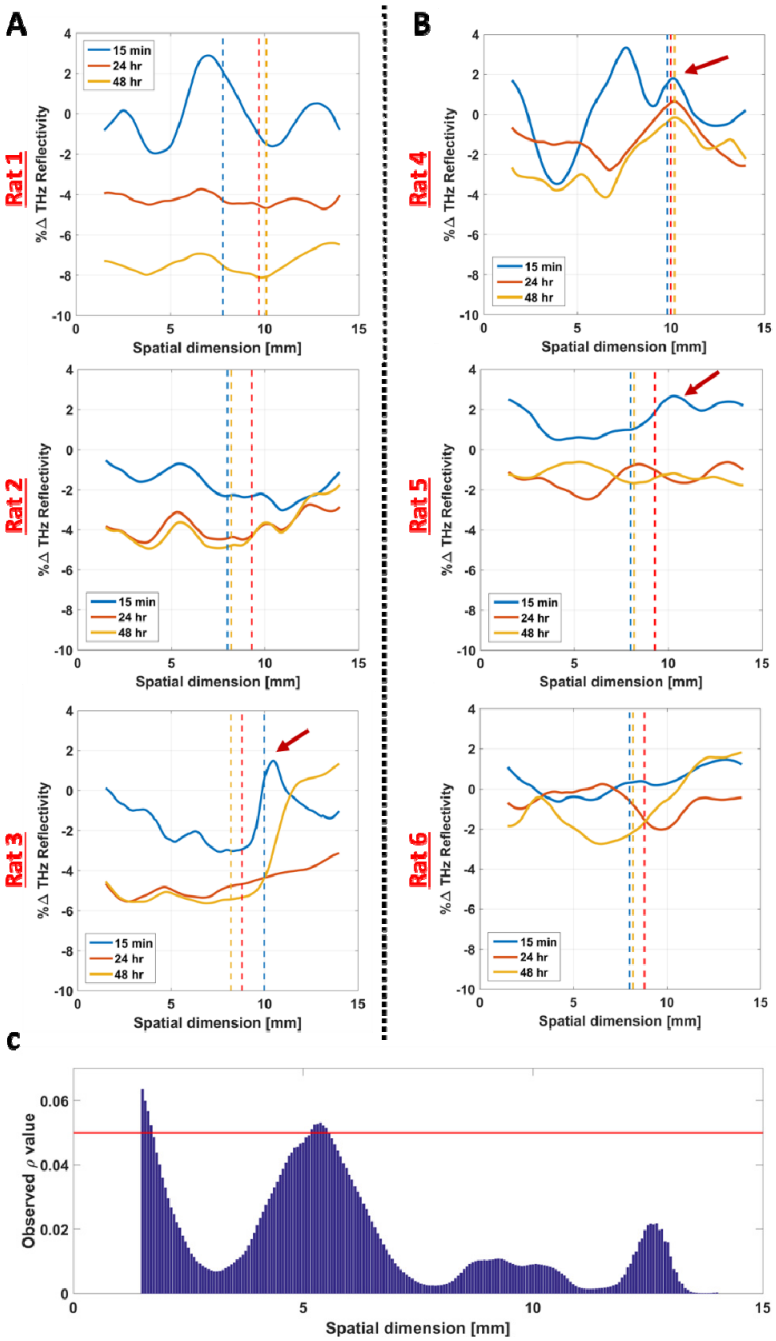

Fig. 5. Spatial THz reflectivity profiles for THz flap image sets. (a) Profiles of %Δ THz reflectivity in excised flaps and (b) bipedicled flaps with respect to pre-surgery values were generated for white contours that segment THz images in Fig. 4. These THz profiles captured the cephalic incision (i.e. dashed vertical lines), flap region (i.e. left of incision), and non-traumatized tissue (i.e. right of incision) of tissue flaps at 15min, 24hr, and 48hr post-operation. All red arrows denote increased THz reflectivity due to the presence of blood immediately following surgery, a confounder to THz contrast. (c) Pixel-by-pixel differences in THz reflectivity between both flap models at 24hr following surgery were confirmed to be statistically significant ($p < 0.05$, the solid red line) across the entire length of the white contour (i.e. x-axis) using an independent student *t*-test.

Biomedical Optics EXPRESS

for rat 1, the drop in reflectivity is more pronounced at 48 hr. The tissue flap texture and topography also drastically change by 7 days postoperatively in this flap failure model. These factors, therefore, begin to slightly confound contrast observed in THz images of all excised flaps at this time point. Because clinical acute assessments of flap viability are typically performed for 48 hours post-operatively, unusual THz contrast observed at 7days post-surgery in excised flaps is clinically irrelevant, and therefore can be ignored. As expected, %Δ THz reflectivity of non-traumatized tissue adjacent to all excised flaps (i.e. right of the dotted vertical line in Fig. 5(a)) approached baseline values (0%). This result is particularly evident in both rats 2 and 3. By comparison, most %Δ THz reflectivity for both the flap region and adjacent non-traumatized tissue in bipedicled flaps either remained within the same reflectivity neighborhood or approached that at pre-surgery (0%) at 24hr following surgery. This result is particularly apparent in THz reflectivity plots for rat 5 and rat 6, neither of which dip below –2%Δ in reflectivity. This behavior persists at 48hr and 7days post-surgery, as there are no gross topographical changes expected in a tissue survival model. Irregularities in THz contrast, such as reduced %Δ THz reflectivity in the form of troughs for plots at 48hr for rat 4 and rat 6, were likely explained by suboptimal coupling of tissue flaps with the dielectric window, irregular incision geometries, as well as differences in perfusion due to non-uniform flap surgery.

Because 24hr post-surgery is clinically more important for flap assessment, an independent Student *t*-test was performed to assess differences in reflectivity between a flap failure model and flap survival model at this time point (see Fig. 5(c)). Such an analysis has important clinical implications, as gross changes in tissue flap viability are typically visually apparent 48hr following surgery. In Fig. 5(c), the y-axis describes the significance value (rho) of an independent t-test performed between the %Δ THZ reflectivity profiles of all bipedicled flaps (n = 3) and excised flaps (n = 3) at 24hr post-surgery in Fig. 5(a) and 5(b). As previously explained, %Δ THz reflectivity profiles at 24hr represent the pixel-by-pixel reflectivity difference between the pre-operative image and post-surgery image at 24hr along the white line contour. The x-axis in Fig. 5(c) represents the spatial dimension of this contour. Differences in THz reflectivity at 24hr post-surgery between both flap viability models are statistically significant (i.e. $p < 0.05$, denoted by the horizontal red line) along the entire length of the contour. Moreover, this statistically significant variation in THz reflectivity between a flap survival and flap failure model is observed 24hr prior to gross changes in tissue viability using clinical inspection alone.

7.2 Gross examination

Surviving surface areas in each flap viability model were markedly different as shown in Fig. 6. Clinical evaluation of bipedicled flap tissue revealed no signs of ischemia (i.e. cyanosis) and minimal change in skin pliability, all indicative of a surviving flap. Contraction of the cephalic and caudal incisions by Day7 suggested optimal wound healing likely due to neovascularization and metabolic support from the lateral pedicles. The survival area was estimated to be 100% by two independent observers (JKA and RJ). Conversely, the excised flaps displayed progressive necrosis over 7 days. At 24hr, the flaps appeared grossly absent of congestion or cyanosis, with no clear demarcation being evident between viable and nonviable tissue. By 48hr, tissue contraction and cyanosis began to appear near the peripheral segments and on examination accounted for 30%, 40%, and 25% of the flap area in rat 1, rat 2, and rat 3, respectively. This necrosis continued, and by Day7, a well-defined demarcation line between viable and nonviable tissue was evident. The surviving surface area of the myofascial flap was estimated to be ~0%, 10%, and 20% for rat 1, rat 2, and rat 3, respectively.

Biomedical Optics EXPRESS

7.3 Histological assessment

Histological verification of tissue viability of both bipedicled and excised flaps was necessary, as this was the first pilot study to investigate these tissue flap types with the reported dimensions; although a 2.5 cm x 2.5 cm bipedicled flap and excised flap were *hypothesized* to result in a survival and failure model, respectively, there is no confirmation of this result in the literature. Figure 4 shows histological evaluation of tissue sections from both flap models

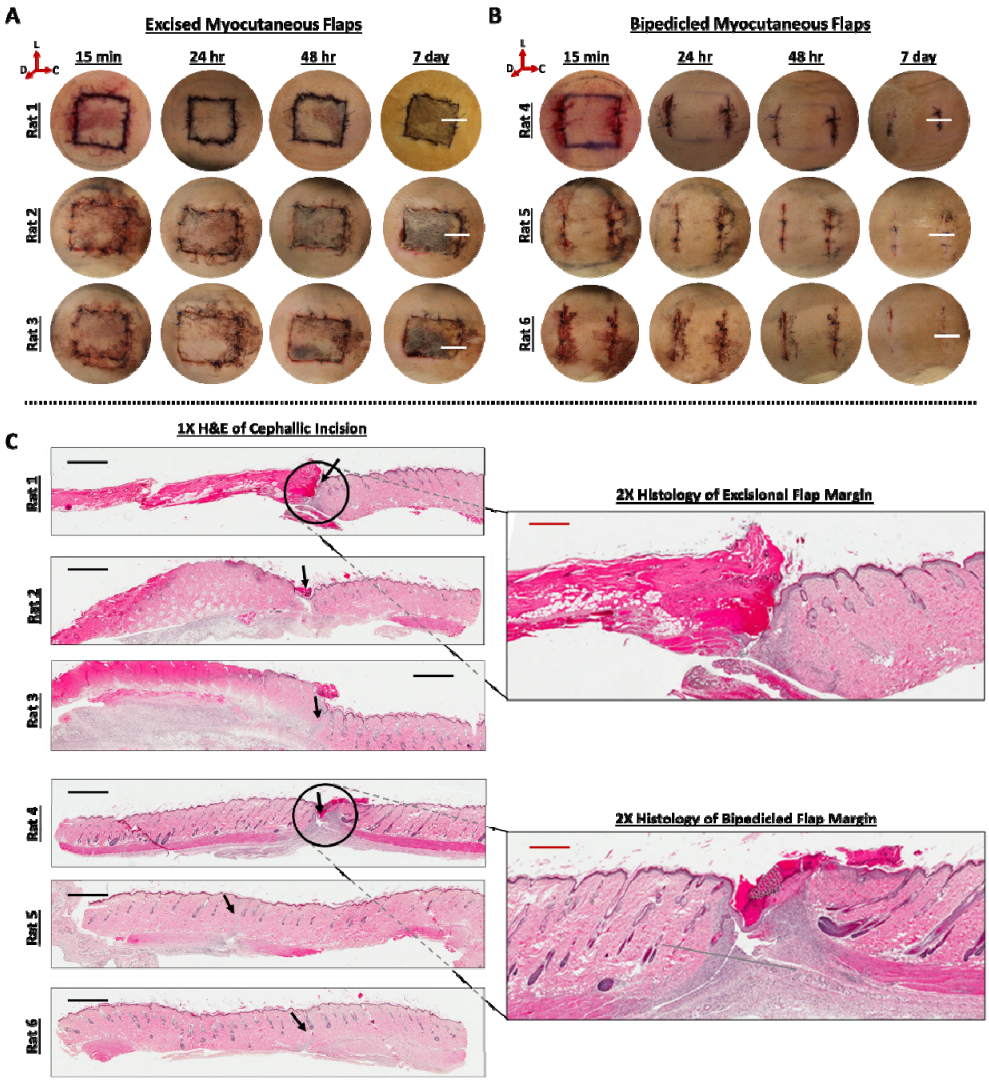

Fig. 6. Clinical and histological assessment of flap viability. Post-operative visual surveillance of (a) excised flaps and (b) bipedicled flaps over 7 days. "L," "D," and "C" correspond to directions in Fig. 2. (c) 1X and 2X representative hematoxylin and eosin (H&E) staining for tissue flap margins spatially map to the cephalic incision at day 7, demarcated by white horizontal lines in the visible imagery. In the H&E image, flap tissue and non-traumatized tissue lie to the left and right of the incision site (denoted by a black arrow), respectively. Necrotic tissue appears dark magenta in the H&E stain. The black scale bar and red scale bar represent ~1 mm and ~450 µm, respectively.

Biomedical Optics EXPRESS

confirmed viability results that were evident grossly at 7 days following surgery. A blinded pathologist identified all histological sections from cephalic incisions of the excisional flaps as necrotic (see Fig. 4(c)). Severe, full thickness necrosis of the skin and underlying muscle layers as well as the loss of dermal papilla and sebaceous glands were captured by hypereosinophilia in hematoxylin and eosin (H&E) stained sections, delineating a clear demarcation between the non-traumatized viable tissue. Neovascularization and early collagen deposition were only compromised and apparent in the adjacent, non-injured tissue.

In contrast, caudal and cephalic segments of bipedicled flaps were all completely viable (~0% necrosis) on histological evaluation (see Fig. 4(c)). Both non-injured and flap segments were characterized by intact skin and muscle layers, subcutaneous follicles, and glands. While absent in the samples of the excised flaps, early signs of wound healing, specifically granulation tissue and chronic inflammation, were apparent at the incision margin (denoted by black arrow).

8. Discussion

Since water constitutes ~70% of the skin weight and the THz frequency dielectric constant of water is significantly higher than that of non-water constituents, increases in THz reflectivity are assumed to be approximately positively correlated to increases in TWC of tissue, such as a flap [13,16,19,24]. In this way, variation in TWC of dorsal tissue flaps can be monitored non-invasively with reflective THz imaging as a function of time and location to determine tissue viability. It is important to note that THz imaging furnishes a 2D refection image of TWC *contrast* rather than an *absolute* measurement of TWC. Because THz-based visualization of *variation* in TWC is both early and accurate, this technique is more clinically attractive than more costly, difficult, and lengthy estimations of *absolute* TWC. For instance, magnetic resonance imaging is one of the few techniques used to determine the fraction of protons available in tissue, however, its cost and limited portability make it inappropriate for TWC characterization in patients, especially critical patients.

As originally hypothesized, *in vivo* THz imaging measurements indicate that TWC of an excised flap and bipedicled flap model, determined to have low and high tissue viability, respectively, is markedly different. Moreover, variation in TWC between both flap models is evident as early as 24 hr post-operatively. Following surgical elevation of excised flaps, THz TWC contrast at the cephalic incision site is significantly lower than that of the pre-elevation value (see Fig. 4(a) and Fig. 5(a)). TWC contrast observed in THz imagery at this site continues to progressively decline for the remainder of the 7-day observation period.

Spatiotemporal variations in TWC contrast in THz imagery of the excisional flap model are consistent with both clinical and histological assessments of flap viability. As shown in Fig. 6(a), there are few visual signs of desiccation or abnormalities (i.e. edema) observed within excised flap tissue 24 hr after the surgical procedure has been completed. Difficulty in visual assessment of edema arises because fluid build-up, that is perceived clinically as an increase in tissue volume, is only visually apparent after tissue volume has doubled [10]. At this same time point, however, the TWC THz map has clearly identified those regions of tissue that were insufficiently hydrated. Since adequate perfusion of the dermal plexus is essential to sustain the functional and structural viability of the skin, it is expected that severely dehydrated tissues will gradually proceed to ischemia, and finally necrosis [25]. This progression is grossly observed 48 hr after surgery as well as confirmed histologically on Day 7 in Fig. 6(a); skin flaps rely on the underlying vascularity of the bed for adequate TWC and nutrients, and therefore wounds that are poorly vascularized, as in the case of an excised injury, will not support the flap [26].

Conversely, THz TWC contrast across a bipedicled flap remains similar to that at pre-surgery as shown in Fig. 5(b). This TWC result is likely due to survival mechanisms characteristic to flaps containing pedicles, or an intact blood supply:

Biomedical Optics EXPRESS

1) *Plasmatic imbibition* — Initially, skin flaps passively absorb nutrients in the wound bed by diffusion. Both the bipedicled flap and excised flap received rudimentary nutrition in this manner. However, in the excised flap this mechanism was the sole source of tissue nutrients, while the bipedicled flap retained its dermal plexus for tissue perfusion. It is likely that the nutritional demand of the excised flap proved to be in excess of the nutritional supply by plasmatic imbibition resulting in subsequent tissue ischemia and necrosis, and therefore reduced TWC, by 24 hours (see Fig. 5) [27–29].

2) *Inosculation* — By day 2 to 3, the cut ends of the vessels on the underside of the flap dermis begin to form connections with those of the wound bed. This likely explains the observed rise in THz reflectivity, or TWC, towards baseline for bipedicled flaps at 48 hr in Fig. 5(b). After this point, new blood vessels grow (i.e. angiogenesis) into the flap and the tissue becomes fully vascularized [27].

Clinical and histological evaluation of tissue viability of the bipedicled flaps support this finding. Collectively, THz visualization of differences in flap TWC enables detection of flap status 24 hr prior to clinical assessment and reported imaging methods (i.e. laser Doppler imaging), and, thus, may afford important implications in a number of areas of our research, including edema monitoring in wounds and skin evaluation [15,16]. Specifically, in clinical cases when a pre-evaluation THz scan of TWC is typically unavailable, early detection of TWC changes with respect to the neighboring uninjured tissue could enable expedited surgical re-exploration and potential salvage of failing tissue flaps prior to irreversible ischemia.

There are several key experimental points that warrant additional investigation. From a clinical vantage point, the use of windows for THz flap assessment is factor that affects the accuracy of THz measurement and is a practical barrier to non-contact, *in vivo* medical translation of this technology. Concerns include physical perturbation of the wound and pressure exertion that may change TWC image contrast. Although windowless flap assessment is ideal, low-loss dielectric windows are necessary in THz imaging to minimize confounding effects from non-planar geometries and respiratory motion *in vivo*. Both high and low dielectric substrates, including quartz, sapphire, and thin stretched Mylar, are commonly used to flatten the imaging target. During our THz flap imaging study, we employed a thin Mylar window and observed that flexibility of the film may not have sufficiently eliminated confounding contributions from irregular surface features. In future studies, we plan to test the repeatability and accuracy of THz imaging using 500 μm quartz, a more rigid substrate.

Next, flap dimensions and how this may potentially change THz TWC contrast must be explored; the surface area to nutrient ratio of larger excised flaps is greater, which may lead to earlier necrosis. Because tissue flaps also vary in thickness, depending on where the flap is located on the body, electromagnetic modeling may offer more insight into how THz TWC contrast varies as a function of skin thickness. Additionally, significant TWC findings observed in this preliminary study lay the groundwork for future serial studies in which biopsies can be performed at 24hr and 48hr to investigate the predictive power of THz imaging for flap viability assessment. Inclusion of these experimental design parameters, coupled with existing rapid and noninvasive THz imaging, may lend reflective THz sensing as a powerful augmentation to the standard clinical assessment of tissue.

9. Conclusion

Large soft tissue defects resultant from oncologic surgery require tissue flap reconstruction to mitigate postoperative morbidity and mortality. Perfusion is often used to predict the viability of these flaps. Because TWC is a significant confounder to early perfusion-based assessments, this work set out to use reflective THz imaging, a non-invasive TWC sensing method, to evaluate the viability of myocutaneous dorsal flaps in an *in vivo* rat model.

Biomedical Optics EXPRESS

Reflective THz imaging detects variation in TWC between a histologically confirmed flap failure model and flap survival model 24 hr prior to clinical inspection alone. This ability to rapidly and non-invasively assess flap viability by monitoring changes in TWC may enable earlier and more successful intervention in reconstructive surgery.

Funding

This work is supported by the National Institute of Biomedical Imaging and Bioengineering (NIBIB) Grant# R21EB015084 and Grant# R21EB016896.